

Design and Analysis of LoS MIMO Systems with Uniform Circular Arrays

Yuri Jeon, Gye-Tae Gil, *Member, IEEE*, and Yong H. Lee, *Senior Member, IEEE*

Abstract—We consider the design of a uniform circular array (UCA) based multiple-input multiple-output (MIMO) system over line-of-sight (LoS) environments in which array misalignment exists. In particular, optimal antenna placement in UCAs and transceiver architectures to achieve the maximum channel capacity without the knowledge of misalignment components are presented. To this end, we first derive a generic channel model of UCA-based LoS MIMO systems in which three misalignment factors including relative array rotation, tilting and center-shift are reflected concurrently. By factorizing the channel matrix into the singular value decomposition (SVD) form, we demonstrate that the singular values of UCA-based LoS MIMO systems are *independent* of tilting and center-shift. Rather, they can be expressed as a function of the *radii product-to-distance ratio* (RPDR) and the angle of relative array rotation. Numerical analyses of singular values show that the RPDR is a key design parameter of UCA systems. Based on this result, we propose an optimal design method for UCA systems which performs a one-dimensional search of RPDR to maximize channel capacity. It is observed that the channel matrix of the optimally designed UCA system is close to an orthogonal matrix; this fact allows channel capacity to be achieved by a simple zero-forcing (ZF) receiver. Additionally, we propose a low-complexity precoding scheme for UCA systems in which the optimal design criteria cannot be fulfilled because of limits on array size. The simulation results demonstrate the validity of the proposed design method and transceiver architectures.

Index Terms—Uniform circular array, line-of-sight channel, array misalignment.

I. INTRODUCTION

DUE to the potential in fixed wireless applications such as cellular backhaul, line-of-sight (LoS) multiple-input multiple-output (MIMO) communication systems with fixed transmitter and receiver locations have been proposed [1]–[12]. In these systems, the LoS MIMO channel is nearly stationary and can be assumed to be deterministic. To provide the high data rates required for such applications, LoS MIMO systems exploit spatial multiplexing gains attained by appropriate spacing between antenna elements. It has been shown that LoS MIMO systems can achieve a full multiplexing gain through the optimization of antenna placement [2]–[9]. In particular, the orthogonality conditions that make the columns of LoS MIMO channel matrices orthogonal, are derived in

terms of the carrier wavelength, array size, and communication range. Furthermore, sensitivity to deviations caused by small misalignments, such as rotations, tilts, or translations has been analyzed [4]–[9]. These results have been derived mostly for uniform linear arrays (ULAs) [4]–[7] and uniform rectangular arrays (URAs) [8]–[9].

Recently, LoS MIMO communication systems with uniform-circular-arrays (UCAs) have been drawing attention due to their advantages over ULAs and URAs [10]–[15]: a salient feature of a UCA-based LoS MIMO system is that its channel matrix can be modeled as a circulant matrix [10]–[12]; thus, the channel can be diagonalized by employing a discrete Fourier transform (DFT) precoder and an inverse DFT (IDFT) combiner. This property can simplify the design and implementation of UCA-based LoS MIMO systems, and it allows us to regard UCA-based LoS MIMO systems as a candidate scheme for realizing orbital-angular momentum (OAM) transmission [12], [16]–[19]. However, these systems have not been fully investigated, and their use for practical applications is limited. The orthogonality condition for optimal antenna spacing has been derived only for UCAs with three or four antenna elements [11]. In addition, the asymptotic analysis in [10] indicates that a UCA-based MIMO channel can hardly satisfy the orthogonality condition and has jagged singular values, where some of them are too small to be used for signal transmission. In other words, the condition number of the channel matrix can be large, and it is difficult to exploit the full multiplexing gain. To overcome these difficulties, an optimal design method which is a process of finding the optimal radii of UCAs to maximize channel capacity was presented [13]. However, all of the research efforts consider only a scenario in which the transmitter (Tx) and the receiver (Rx) UCAs are perfectly aligned to each other.

While there has been a lack of discussion on the optimal design criteria of UCA systems under array misalignment, it has traditionally been believed that misalignments on UCAs should be compensated to obtain high performance gain. In this regard, channel models of misaligned UCA systems and methods to compensate for those misalignments have been developed [14], [19]. Channel models of center-shifted and tilted UCA systems were presented in [14] and [19], respectively, but a generic channel model that considers all kinds of misalignment concurrently has not yet been developed. Moreover, the misalignment compensation methods of [14] and [19] leverage the phase deviation of channel gain caused by misalignments, but its estimation method, which is an important issue for realization, was not presented. In practice, it is challenging to estimate misalignment angles

This work has been submitted to the IEEE for possible publication. Copyright may be transferred without notice, after which this version may no longer be accessible.

Y. Jeon and Y. H. Lee are with the School of Electrical Engineering, Korea Advanced Institute of Science and Technology, Daejeon 34141, Korea (e-mail: yuri0703@kaist.ac.kr; yohlee@kaist.ac.kr).

G. T. Gil is with the Institute for Information Technology Convergence, Korea Advanced Institute of Science and Technology, Daejeon 305-701, South Korea (e-mail: gategil@kaist.ac.kr).

when they are small or vary rapidly. Therefore, in-depth analysis of sensitivity to misalignment and finding a way to implement UCA systems without estimating or compensating misalignment components are required.

In this work, we develop an optimal design method for a UCA system under array misalignment and present transceiver architectures that achieve the channel capacity without estimating or compensating misalignment components. Here, we first present a generalized channel model of a misaligned UCA system in which all kinds of misalignments including tilting, center-shift, and array rotation, are taken into account. Then, it is shown that the singular values of the misaligned UCA system are independent of tilting and center-shift, but can be expressed as a function of the *radii product-to-distance ratio* (RPDR) and the angle of relative array rotation. Further numerical analyses verify that the singular values are robust to array rotation, but fluctuate with the RPDR. These findings indicate that the RPDR is the key parameter for designing UCA systems. Based on this observation, we developed an optimal design method for UCA systems that performs a one-dimensional search for the RPDR to maximize the channel capacity. It is observed that the channel matrix of the misaligned UCA system is close to an orthogonal matrix when the optimal design criterion is satisfied; therefore, the maximum channel capacity can be achieved by a simple zero-forcing (ZF) receiver. In addition, we develop a low-complexity precoding scheme for a UCA system in which the optimal RPDR value cannot be fulfilled due to limits on array size. The proposed precoding scheme consists of approximated power allocations, which can be implemented only by the information of the communication distance, and a codebook-based precoding framework where the codebook is designed by quantized angles of center-shift to avoid estimation of misalignment angles. The results indicate that the proposed precoding scheme almost achieves the channel capacity with a small feedback overhead; thus, it can be a useful alternative to an optimal precoder that requires either estimation and feedback of misalignment angles or full channel-state information.

The remainder of this paper is organized as follows. Section II presents the channel model of a misaligned UCA system in which three types of misalignments, i.e., rotation, tilting and center-shift, are taken into account. In Section III, singular value analyses are performed, and the optimal design method of the misaligned UCA system is presented. The design of a precoder for non-optimal UCA systems is presented in Section IV, and simulation results demonstrating the validity of the proposed design method and transceiver architectures are presented in Section V. Finally, Section VI presents the conclusion.

Notations: Bold upper-case \mathbf{A} denotes a matrix and bold lower-case \mathbf{a} denotes a vector. Superscripts \mathbf{A}^T and \mathbf{A}^H denote the transpose and the conjugate transpose of a matrix \mathbf{A} , respectively, and a^* denotes the complex conjugate of a complex number a . The $(n, m)^{th}$ entry and the k th column of a matrix \mathbf{A} are denoted as $a(n, m)$ and $\mathbf{A}(:, k)$, respectively, and $\text{diag}(a_1, \dots, a_N)$ indicates a diagonal matrix whose diagonal entries are given by $\{a_1, \dots, a_N\}$. The matrix obtained by taking the magnitudes of the entries of \mathbf{A} is denoted as

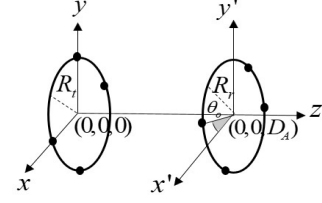


Fig. 1. Perfectly aligned UCA system when $N_s = 4$.

$|\mathbf{A}|$ (the $(n, m)^{th}$ entry of $|\mathbf{A}|$ is equal to $|a(n, m)|$), and \mathbf{I}_N denotes the N -dimensional identity matrix. The matrices \mathbf{R}_{θ}^{xy} , \mathbf{R}_{θ}^{xz} and \mathbf{R}_{θ}^{yz} are rotation matrices representing the rotation on the xy -plane about the z -axis, on the xz -plane about the y -axis, and the on yz -plane about the x -axis, respectively. For example,

$$\mathbf{R}_{\theta}^{xz} = \begin{bmatrix} \cos \theta & 0 & -\sin \theta \\ 0 & 1 & 0 \\ \sin \theta & 0 & \cos \theta \end{bmatrix}.$$

II. SYSTEM MODEL

In this section, we present a system model for misaligned UCA systems. It is assumed, without loss of generality, that misalignments are caused by the misplacement of an Rx UCA, given a well-positioned Tx UCA. The misplacement is modelled by the rotation, tilting and center-shift of an Rx UCA. We shall consider these misplacement models one by one, and then present a general model that jointly considers all three types of misplacements. The misalignment model presented in this section is an extension of the model introduced in [14] that considers rotation and center-shift.

A. Aligned UCAs with Rotation

We consider a UCA system over an LoS channel that employs UCAs with N_s antenna elements at the transmitter (Tx) and the receiver (Rx). The radii of the Tx and Rx UCAs are denoted as R_t and R_r , respectively. For the aligned UCAs, we assume that the Tx UCA is located on the xy -plane and is centered at the coordinate $(x, y, z) = (0, 0, 0)$; the Rx UCA is located on the xy -plane, which is parallel to the xy -plane, and centered at $(x, y, z) = (0, 0, D_A)$, where $D_A \gg R_t$ and R_r . The Tx UCA is assumed to be fixed, and without loss of generality, the first Tx antenna element is located on the x -axis. The coordinates of the m^{th} Tx antenna are given by $(R_t \cos \theta_m, R_t \sin \theta_m, 0)$ for $\theta_m = 2\pi m/N_s$ and $m \in \{1, \dots, N_s\}$. For the Rx UCA, we allow rotation by θ_o about the z -axis, where $-\pi/N_s \leq \theta_o \leq \pi/N_s$ (Fig. 1). The coordinates of the n^{th} Rx antenna after rotation, denoted as $(x_{\theta_o}, y_{\theta_o}, z)$, are given by

$$\begin{aligned} [x_{\theta_o}, y_{\theta_o}, z]^T &= \mathbf{R}_{\theta_o}^{xy} [R_r \cos \theta_n, R_r \sin \theta_n, D_A]^T \\ &= [R_r \cos(\theta_n + \theta_o), R_r \sin(\theta_n + \theta_o), D_A]^T. \end{aligned} \quad (1)$$

where $\mathbf{R}_{\theta_o}^{xy}$ is the rotation matrix representing the rotation on the xy -plane about the z -axis, $\theta_n = 2\pi n/N_s$, and $n \in$

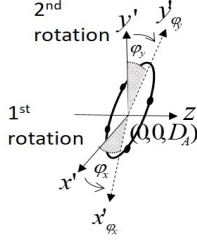


Fig. 2. Tilting modeled as a cascade of two rotations.

$\{1, \dots, N_s\}$. The distance between the m^{th} Tx antenna and the n^{th} Rx antenna, denoted as $\tilde{d}_A(n, m)$, is given by

$$\tilde{d}_A(n, m) = \{D_A^2 + R_t^2 + R_r^2 - 2R_t R_r \cos(\theta_n - \theta_m + \theta_o)\}^{\frac{1}{2}}. \quad (2)$$

Because $D_A \gg R_t$ and R_r , ignoring the approximation errors, $\tilde{d}_A(n, m)$ can be rewritten as

$$\tilde{d}_A(n, m) = D_A - \frac{R_t R_r}{D_A} \cos(\theta_n - \theta_m + \theta_o). \quad (3)$$

B. Modeling Rx UCA Tilting

Referring to Fig. 2, the Rx UCA tilting can be represented as a cascade of two rotations: the UCA rotation about the x' -axis by the angle φ_y followed by the rotation about the y'_{φ_y} -axis by the angle φ_x . The first rotation represents the tilt to the $x'z$ -plane, and the second rotation represents the tilt to the $y'z$ -plane. Because the $x'y'$ -plane is parallel to the xy -plane (Fig. 1), the coordinates of an antenna on the Rx UCA after the first rotation are given by $(x, y_{\varphi_y}, z_{\varphi_y})$, where $[x, y_{\varphi_y}, z_{\varphi_y}]^T = \mathbf{R}_{\varphi_y}^{xy}[x, y, z]^T$. The coordinate after the second rotation is given by $(x_{\varphi_x}, y_{\varphi_y}, z_{\varphi_x, \varphi_y})$, where $[x_{\varphi_x}, y_{\varphi_y}, z_{\varphi_x, \varphi_y}]^T = \mathbf{R}_{\varphi_x}^{xz}[x, y_{\varphi_y}, z_{\varphi_y}]^T$. Combining these results, the coordinate after the two types of rotations (or tilting) is given by

$$[x_{\varphi_x}, y_{\varphi_y}, z_{\varphi_x, \varphi_y}]^T = \mathbf{R}_{\varphi_x}^{xz} \mathbf{R}_{\varphi_y}^{xy} [x, y, z]^T. \quad (4)$$

When both the rotation considered in (1) and the tilting in (4) occur, the UCA coordinate is given by $(x_{\theta_o, \varphi_x}, y_{\theta_o, \varphi_y}, z_{\varphi_x, \varphi_y})$ where

$$[x_{\theta_o, \varphi_x}, y_{\theta_o, \varphi_y}, z_{\varphi_x, \varphi_y}]^T = \mathbf{R}_{\varphi_x}^{xz} \mathbf{R}_{\varphi_y}^{xy} [x_{\theta_o}, y_{\theta_o}, z]^T \quad (5)$$

for $(x_{\theta_o}, y_{\theta_o})$ in (1).

C. Modeling Rx UCA Center Shift

Fig. 3 illustrates the Rx UCA center-shift. Here the origin $(0, 0, 0)$ and (c_x, c_y, c_z) represent the coordinates of the centers of the Tx and Rx UCAs, respectively. The center of the Rx UCA is supposed to be located at the coordinate $(0, 0, D_A)$, but it is shifted to (c_x, c_y, c_z) because of misalignment. For convenience, we define a vector $\mathbf{c} = [c_x, c_y, c_z]^T$ from the origin to the center of the Rx UCA. The magnitude of \mathbf{c} is equal to D , which is the distance between the centers of the Tx and Rx UCAs. The direction of center-shift can be represented by two angles: the polar angle measured from the z -axis is denoted by ϕ_{cs} , and the azimuthal angle of the orthogonal

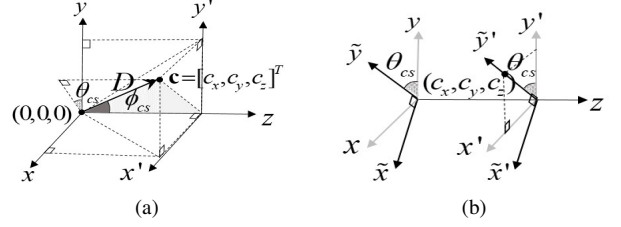


Fig. 3. (a) Modeling the center shift. Ideally, the center is supposed to be located at $(0, 0, D_A)$, but it is shifted to (c_x, c_y, c_z) due to misalignment. (b) Rotating the $x'y'$ -plane by θ_{cs} so that (c_x, c_y, c_z) is located on the \tilde{y}' -axis.

projection of \mathbf{c} on the xy -plane measured from the y -axis is denoted by θ_{cs} . To represent the coordinate change caused by the center-shift using a single rotation matrix, we introduce a new coordinate system, $(\tilde{x}, \tilde{y}, z)$, where the \tilde{x} - and \tilde{y} -axes are the axes obtained by rotating the x - and y -axes by θ_{cs} about the z -axis. In the same way, we also define the \tilde{x}' - and \tilde{y}' -axes from the x' - and y' -axes. Then the center of the Rx UCA is located on the \tilde{y}' -axis as shown in Fig. 3(b), and its coordinates are succinctly represented as follows.

Lemma 1. *In the new coordinate system $(\tilde{x}, \tilde{y}, z)$, the center of the Rx UCA is located at $(0, D \sin \phi_{cs}, D \cos \phi_{cs})$.*

Proof. The coordinates of the center of the new coordinate system are given by $(\tilde{c}_x, \tilde{c}_y, c_z)$ where $[\tilde{c}_x, \tilde{c}_y, c_z]^T = \mathbf{R}_{\theta_{cs}}^{xy}[c_x, c_y, c_z]^T = [0, \sqrt{c_x^2 + c_y^2}, c_z]^T = [0, D \sin \phi_{cs}, D \cos \phi_{cs}]^T$. Here, the 2nd and 3rd equalities follow from the facts that $\cos \theta_{cs} = \frac{c_y}{\sqrt{c_x^2 + c_y^2}}$, $\sin \theta_{cs} = \frac{c_x}{\sqrt{c_x^2 + c_y^2}}$, and $\sqrt{c_x^2 + c_y^2} = D \sin \phi_{cs}$ (Fig. 3(a)). In addition, $c_z = D \cos \phi_{cs}$. This completes the proof. \square

D. Modeling concurrent misalignments

Without loss of generality, we can model the Rx UCA with all three types of misalignments, rotation, tilting and center shift, as follows. The Rx UCA is rotated and tilted at the origin and then shifted so that it is centered at (c_x, c_y, c_z) . From (5), the coordinate of the n^{th} Rx antenna after all three misalignments, denoted as (a_x^n, a_y^n, a_z^n) can be written as

$$\begin{aligned} [a_x^n, a_y^n, a_z^n]^T &= \mathbf{c} + \mathbf{R}_{\varphi_x}^{xz} \mathbf{R}_{\varphi_y}^{xy} \mathbf{R}_{\theta_o}^{xy} [R_r \cos \theta_n, R_r \sin \theta_n, 0]^T \\ &= \mathbf{c} + \mathbf{R}_{\varphi_x}^{xz} \mathbf{R}_{\varphi_y}^{xy} \\ &\quad \times [R_r \cos(\theta_n + \theta_o), R_r \sin(\theta_n + \theta_o), 0]^T. \end{aligned} \quad (6)$$

In the new coordinate system $(\tilde{x}, \tilde{y}, z)$ considered in Lemma 1, (6) is rewritten as follows.

Lemma 2. *In the new coordinate system $(\tilde{x}, \tilde{y}, z)$, the coordinate of the n^{th} Rx antenna, denoted as $(a_{\tilde{x}}^n, a_{\tilde{y}}^n, a_z^n)$, is given by*

$$\begin{aligned} [a_{\tilde{x}}^n, a_{\tilde{y}}^n, a_z^n]^T &= \mathbf{R}_{\theta_{cs}}^{xy} [a_x^n, a_y^n, a_z^n]^T \\ &= \begin{bmatrix} R_1 \cos(\theta_n - \alpha_1) \\ D \sin \phi_{cs} + R_2 \cos(\theta_n - \alpha_2) \\ D \cos \phi_{cs} + R_3 \cos(\theta_n - \alpha_3) \end{bmatrix}, \end{aligned} \quad (7)$$

where $R_i = R_r \sqrt{b_{i1}^2 + b_{i2}^2}$, $\alpha_i = \tan^{-1}(\frac{b_{i2}}{b_{i1}}) - \theta_o$ and b_{ij} is the $(i, j)^{th}$ elements of $\mathbf{R}_{\theta_{cs}}^{xy} \mathbf{R}_{\varphi_x}^{xz} \mathbf{R}_{\varphi_y}^{yz}$.

The result in (7) can be obtained by directly calculating $\mathbf{R}_{\theta_{cs}}^{xy} [a_x^n, a_y^n, a_z^n]^T$. The coordinate of the m^{th} Tx antenna in the new coordinate system is given by $(R_t \cos \theta'_m, R_t \sin \theta'_m, 0)$ where $\theta'_m = \theta_m + \theta_{cs}$. Now the distance between the m^{th} Tx antenna and the n^{th} Rx antenna, $d(n, m)$, can be represented as follows.

Lemma 3. The distance $d(n, m)$ is written as

$$d(n, m) = D \left\{ 1 + f(D, R_t, R_r, \theta_m, \theta_n, \theta_o, \theta_{cs}, \varphi_x, \varphi_y, \phi_{cs}) \right\}^{\frac{1}{2}}, \quad (8)$$

where $f(D, R_t, R_r, \theta_m, \theta_n, \theta_o, \theta_{cs}, \varphi_x, \varphi_y, \phi_{cs})$ is presented in Appendix A.

Proof. See proof in Appendix A. \square

Because $D \gg R_t$ and R_r , $d(n, m)$ can be approximated as

$$\begin{aligned} d(n, m) &= D \left\{ 1 + \frac{1}{2} f(D, R_t, R_r, \theta_m, \theta_n, \theta_o, \theta_{cs}, \varphi_x, \varphi_y, \phi_{cs}) \right\} \\ &= d_A(n, m) - \tau_t(m) + \tau_r(n), \end{aligned} \quad (9)$$

where

$$d_A(n, m) = D - \frac{R_t R_r}{D} \cos(\theta_n - \theta_m + \theta_o), \quad (10)$$

$$\tau_t(m) = R_t \sin(\theta_m + \theta_{cs}) \sin \phi_{cs}, \quad (11)$$

and

$$\begin{aligned} \tau_r(n) &= \frac{R_r^2}{4D} \{ \cos 2(\theta_n - \alpha_1) + \cos 2(\theta_n - \alpha_2) + \cos 2(\theta_n - \alpha_3) \} \\ &\quad + R_2 \cos(\theta_n - \alpha_2) \sin \phi_{cs} + R_3 \cos(\theta_n - \alpha_3) \cos \phi_{cs}. \end{aligned} \quad (12)$$

Note that in (9), $d(n, m)$ is decomposed into three components defined in (10)–(12). Comparing (10) with (3), we can see that $d_A(n, m)$ can be thought of as the distance between the Tx and Rx antennas of an aligned UCA system that only has rotation, such as the one shown in Fig. 1. In (11), $\tau_t(m)$ represents the displacement caused by the center-shift only, while the displacement $\tau_r(n)$ in (12) is caused by all three types of misalignments. The subscripts t and r of $\tau_t(m)$ and $\tau_r(n)$ indicate that m and n are the indices of Tx and Rx antennas, respectively. In what follows, we shall see that the expression for $d(m, n)$ in (9) leads to an efficient representation for the misaligned channel matrix.

Consider the misaligned channel matrix $\mathbf{H} \in \mathbb{C}^{N_s \times N_s}$ whose $(m, n)^{th}$ entry is given by

$$\begin{aligned} h(n, m) &= e^{-j \frac{2\pi}{\lambda} d(n, m)} \\ &= h_A(n, m) \cdot T_t^*(m) \cdot T_r(n) \end{aligned} \quad (13)$$

which is the normalized free-space channel response, where λ is the wavelength of the carrier [2]–[4] and the 2nd equality follows from (9); $h_A(n, m) = e^{-j \frac{2\pi}{\lambda} D} \cdot e^{+j \beta \cos(\theta_n - \theta_m + \theta_o)}$, $T_t(m) = e^{-j \frac{2\pi}{\lambda} \tau_t(m)}$, and $T_r(n) = e^{-j \frac{2\pi}{\lambda} \tau_r(n)}$. Here, $\beta \triangleq \frac{2\pi R_t R_r}{\lambda D}$. The parameter β is referred to as the RPDR. In matrix-form, (13) is rewritten as

$$\mathbf{H} = \mathbf{T}_r \mathbf{H}_A \mathbf{T}_t^H, \quad (14)$$

where $\mathbf{T}_t = \text{diag}[T_t(1), \dots, T_t(N_s)]$ and $\mathbf{T}_r = \text{diag}[T_r(1), \dots, T_r(N_s)]$; the $(n, m)^{th}$ entry of the matrix \mathbf{H}_A is given by $h_A(n, m)$. Because the matrix \mathbf{H}_A is a circulant matrix, (14) can be further decomposed into

$$\mathbf{H} = \mathbf{T}_r \mathbf{Q} \mathbf{\Delta}_A \mathbf{Q}^H \mathbf{T}_t^H, \quad (15)$$

where \mathbf{Q} is the DFT matrix, $\mathbf{H}_A = \mathbf{Q} \mathbf{\Delta}_A \mathbf{Q}^H$, and $\mathbf{\Delta}_A \in \mathbb{C}^{N_s \times N_s}$ is a diagonal matrix. Let $\mathbf{\Delta}_A = \mathbf{S} |\mathbf{\Delta}_A|$, where $\mathbf{S} \in \mathbb{C}^{N_s \times N_s}$ is a diagonal matrix of complex numbers having unit magnitude. Then, the decomposition of the channel matrix \mathbf{H} in (15) leads to the following property.

Property 1. Let $\mathbf{H} = \mathbf{U} \mathbf{\Sigma} \mathbf{V}^H$ represent the SVD of \mathbf{H} , where $\mathbf{U} \in \mathbb{C}^{N_s \times N_s}$ and $\mathbf{V} \in \mathbb{C}^{N_s \times N_s}$ are unitary matrices, and $\mathbf{\Sigma} \in \mathbb{R}^{N_s \times N_s}$ is a diagonal matrix with singular values on its diagonal. Then, the SVD of \mathbf{H} can be written as

$$\begin{aligned} \mathbf{U} &= \mathbf{T}_r \mathbf{Q} \mathbf{S}, \\ \mathbf{\Sigma} &= |\mathbf{\Delta}_A|, \\ \mathbf{V} &= \mathbf{T}_t \mathbf{Q}. \end{aligned} \quad (16)$$

Proof. Because \mathbf{T}_t , \mathbf{T}_r , and \mathbf{S} are diagonal matrices with unit gain ($|\mathbf{T}_t| = |\mathbf{T}_r| = |\mathbf{S}| = \mathbf{I}_{N_s}$), $\mathbf{T}_r \mathbf{Q} \mathbf{S}$ and $\mathbf{T}_t \mathbf{Q}$ are unitary matrices that can serve as the left and right singular matrices of the SVD, and the diagonal entries of $\mathbf{\Sigma}$ are the singular values. Here the singular values are not sorted in order. \square

Because of Property 1, the singular values of \mathbf{H} are identical to those of \mathbf{H}_A ; thus, the capacities of \mathbf{H} and \mathbf{H}_A are the same. Consequently, the singular values and the capacity of the misaligned channel \mathbf{H} are *independent* of the tilting and center-shift angles $\{\theta_{cs}, \phi_{cs}, \varphi_x, \varphi_y\}$. Next we analyze the singular values and obtain the optimal radii of the UCAs maximizing the capacity.

III. CAPACITY AND OPTIMAL DESIGN

A. Singular Value Analysis

Because a singular value of \mathbf{H} , denoted as σ_k for $k \in \{1, 2, \dots, N_s\}$, is equal to that of $\mathbf{H}_A = \mathbf{Q} \mathbf{\Delta}_A \mathbf{Q}^H$, σ_k can be represented as

$$\begin{aligned} \sigma_k &= \left| \mathbf{Q}(:, k)^H \mathbf{H}_A \mathbf{Q}(:, k) \right| \\ &= \left| \sum_{i=0}^{N_s-1} e^{-j \{ \frac{2\pi}{N_s} i(k-1) - \beta \cos(\frac{2\pi}{N_s} i + \theta_o) \}} \right|, \end{aligned} \quad (17)$$

and $\sum_{k=1}^{N_s} \sigma_k^2 = \text{tr}(\mathbf{H}_A \mathbf{H}_A^H) = N_s^2$. The singular value is a function of N_s , θ_o and β . In our analysis, we assume that N_s is given and, whenever necessary, the singular values are denoted as $\sigma_k(\beta, \theta_o)$. The singular values $\sigma_k(\beta, \theta_o)$ exhibit the following characteristics.

Property 2. Suppose that N_s is an even number.

- (a) $\sigma_k(\beta, \theta_o) = \sigma_{N_s+2-k}(\beta, \theta_o)$ for $\{k|2 \leq k \leq N_s\}$.
- (b) $\sigma_1(\beta, \theta_o) \geq \sigma_k(\beta, \theta_o)$ for $\{k|2 \leq k \leq N_s\}$, if $0 \leq \beta \leq \frac{4 \sum_{i=0}^{N_s-1} |\cos(\frac{2\pi}{N_s} i + \theta_o)|}{\pi N_s}$.
- (c) $\lim_{\beta \rightarrow 0} \sigma_1(\beta, \theta_o) = N_s$ and $\lim_{\beta \rightarrow 0} \sigma_k(\beta, \theta_o) = 0$ for $\{k|2 \leq k \leq N_s\}$.
- (d) $\sigma_k(\beta, \theta_o) = \sigma_k(\beta, -\theta_o)$.

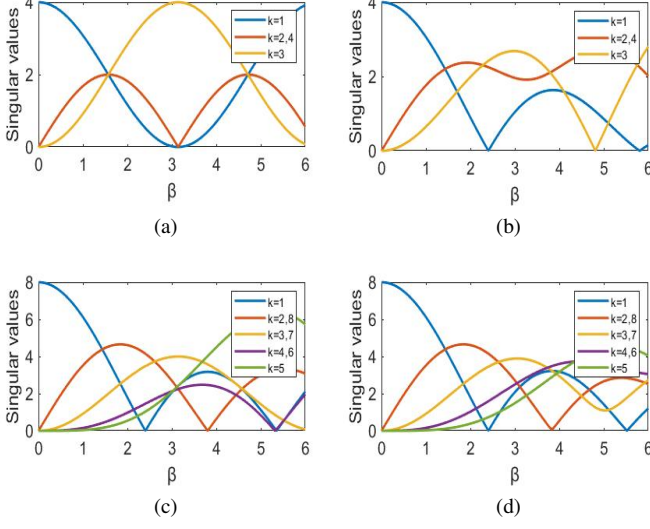


Fig. 4. Singular values against β . (a) $N_s = 4$ and $\theta_o = 0$. (b) $N_s = 4$ and $\theta_o = \pi/(2N_s)$. (c) $N_s = 8$ and $\theta_o = 0$. (d) $N_s = 8$ and $\theta_o = \pi/(2N_s)$.

(e) $\sigma_k(\beta, \theta_o) = 0$ if $k = N_s/2 + 1$ and $\theta_o = \pm\pi/N_s$.

The proofs for Properties 2(a)–(e) are presented in Appendix B. Property 2(a) is an extension of the property in [10] showing that $\sigma_k(\beta) = \sigma_{N_s+2-k}(\beta)$ when $\theta_o = 0$. Because of Property 2(a), there are $N_s/2 + 1$ distinct singular values for given N_s and β . Properties 2(b) and 2(c) indicate that σ_1 becomes dominant as the RPDR, β , decreases. When the radii product $R_t R_r$ is fixed, β decreases as the communication range D increases. Therefore, if a UCA system with small antennas is deployed for long-distance communication, then only one data stream can be transmitted without multiplexing. Property 2(d) indicates that the effects of clockwise and counterclockwise rotations on the singular values are the same. Finally, Property 2(e) shows that $\sigma_{N_s/2+1}(\beta, \theta_o)$ for the $(N_s/2 + 1)^{th}$ eigen-mode becomes zero when $|\theta_o|$ hits its maximum value π/N_s .

Figs. 4 and 5 show the singular value curves against β and θ_o , respectively. These curves confirm Properties 2(a)–(e). The singular values fluctuate as β varies, but they tend to vary slowly for θ_o . In the following subsection, we shall see that the system capacity also fluctuates with β , and we will find the optimal value of β that maximizes the capacity.

B. Optimal Radii of UCAs

In [13], a one-dimensional search process for obtaining the optimal radii of an aligned UCA system, maximizing the spectral efficiency when N_s , λ , and D are given, was proposed. This method searches for the optimal value of the product of R_t and R_r , under the assumption that equal power allocation is adopted. In this subsection, we present an alternative approach to determining the optimal radii. Throughout this subsection, it is assumed that θ_o is fixed. The proposed method assumes the water-filling power allocation and maximizes the capacity; however, it is simpler to implement than the method introduced in [13].

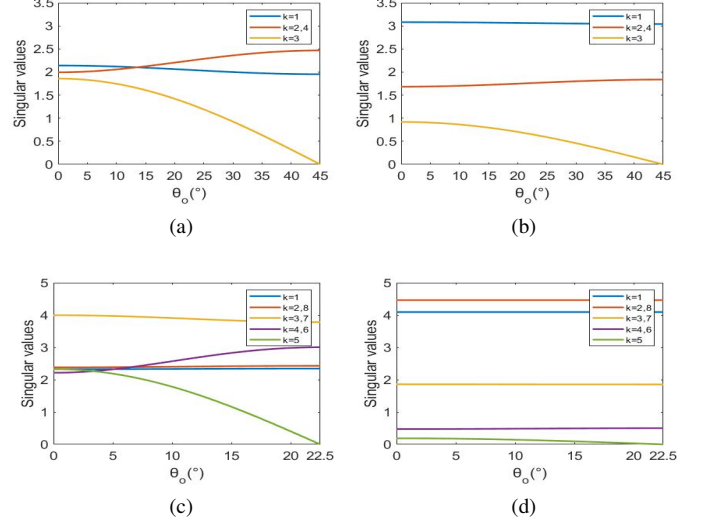


Fig. 5. Singular values against θ_o . (a) $N_s = 4$ and $\beta = 1.5$. (b) $N_s = 4$ and $\beta = 1$. (c) $N_s = 8$ and $\beta = 3.1$. (d) $N_s = 8$ and $\beta = 1.5$.

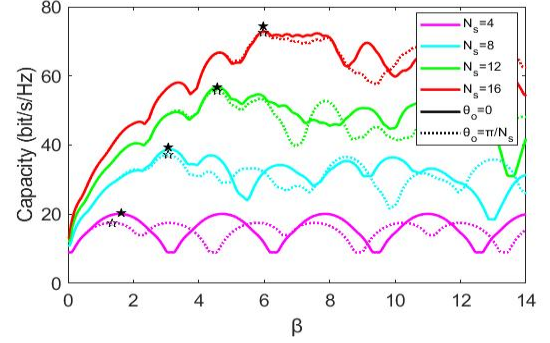


Fig. 6. Capacity curves \mathcal{C}_{N_s} against β when $N_s \in \{4, 8, 12, 16\}$ and $P_T/N_o = 15\text{dB}$. The maximum values \mathcal{C}_{N_s} are marked by \star for $\theta_o = 0$ and \star^\bullet for $\theta_o = \pi/N_s$.

The capacity of a UCA system, denoted as \mathcal{C}_{N_s} , with channel \mathbf{H} corrupted by additive white Gaussian noise (AWGN), is given by

$$\mathcal{C}_{N_s} = \sum_{k=1}^{N_s} \log_2 \left(1 + \frac{p_k \sigma_k^2}{N_o} \right) \quad (18)$$

where $\{p_k\}$ denotes the water-filling power allocations [20]. The proposed scheme is based on the observation that both σ_k and p_k in (18) are functions of N_s and β . This observation holds true because the optimal power allocation $\{p_k\}$ are functions of $\{\sigma_k\}$, which in turn are functions of N_s and β , as shown in (17). Based on this observation, we can search for an optimal RPDR value β^o that maximizes the capacity in (18) when N_s and the signal-to-noise ratio (SNR), P_T/N_o where $P_T = \sum_{k=1}^{N_s} p_k$, are given. The one-dimensional search for finding β^o is straightforward. The search range starts from zero and is reasonably narrow, because $D \gg R_t$ and R_r . In the proposed design, we pre-determine the optimal RPDR β^o values for all $\{N_s, \frac{P_T}{N_o}\}$ values of interest during the initial stage and use them to obtain the optimal radii product $R_t R_r$ when λ and D are given. This two-step process is simpler to

TABLE I
OPTIMAL RPDR VALUES (β°) FOR $N_s \in \{4, 8, 12, 16\}$ AND $\theta_o = 0$.

SNR (dB) \ N_s	4	8	12	16
5	1.57	3.10	4.53	5.98
10	1.51	3.08	4.56	5.97
15	1.54	3.09	4.57	5.98
20	1.54	3.08	4.55	5.98

TABLE II
OPTIMAL RADIUS ($R_t = R_r$) AND THE CORRESPONDING CAPACITY WHEN $N_s \in \{4, 8, 12, 16\}$, $\lambda = 0.004$ METERS (75GHz), $D = 100$ METERS, AND SNR = 15dB.

N_s	4	8	12	16
$R_t(R_r)$ (meters)	0.31	0.44	0.54	0.62
C_{N_s} (bit/s/Hz)	20.11	38.79	56.79	72.88

implement than this proposed in [13], which directly searches for the optimal radii product $R_t R_r$.

Fig. 6 shows the capacity curves C_{N_s} against β , for $0 < \beta \leq 14$, $N_s \in \{4, 8, 12, 16\}$, $\theta_o \in \{0, \pi/N_s\}$, and $P_T/N_o = 15$ dB. When β approaches zero, because of Property 2(c), the capacity of a UCA system in (18) becomes $\log_2(1 + \frac{P_T N_s^2}{N_o}) \approx \log_2(\text{SNR}) + 2\log_2 N_s$. In general, the optimal RPDR, β° , is not unique and we choose the smallest β° from the set of the optimal RPDR values, to minimize the antenna size. Note that the optimal RPDR values maximizing the capacity for $\theta_o = 0$ and π/N_s are almost identical; they are robust to θ_o , and we list only the optimal RPDR values for $\theta_o = 0$ in Table I, which shows β° for $P_T/N_o \in \{5 \text{ dB}, 10 \text{ dB}, 15 \text{ dB}, 20 \text{ dB}\}$. In Table I, the optimal RPDR values for a fixed N_s are almost identical irrespective of the SNR. This happens because the singular values are independent of the SNR, and equal power allocation is almost optimal under a high-SNR regime. Furthermore, as seen in Table I, β° tends to increase linearly with N_s . Therefore, when designing a UCA system for a given D , it is necessary to increase the product $R_t R_r$ in proportion to N_s .

To illustrate UCA systems designed by the proposed method, we design UCA systems with the following parameters: $\lambda = 0.004$ meters (75 GHz), $D = 100$ meters, $R_t = R_r$, SNR = 15 dB, and $N_s \in \{4, 8, 12, 16\}$. The results are shown in Table II. The optimal radius increases with N_s and the capacity gain achieved by increasing both N_s and the radius can be significant.¹

C. Optimal Transceiver of the Optimal UCA System

Table III shows the condition numbers ($\max \sigma_k / \min \sigma_k$) when the RPDR value is optimal and $\theta_o = 0$. When $N_s > 4$, although the singular values are not identical when the RPDR value satisfies the optimal value, the deviation among singular values is reasonably small if the number of antennas is small, e.g., $N_s = 8$, indicating that the column vectors of the

TABLE III
CONDITION NUMBER OF σ_k WHEN $N_s \in \{4, 8, 12, 16\}$ AND $\theta_o = 0$

N_s	4	8	12	16
Condition number ($\max \sigma_k / \min \sigma_k$)	1	1.84	2.42	3.51
$\beta = \beta^\circ$ $\beta = 0.5\beta^\circ$	6.36	22.63	104.53	469.97

channel \mathbf{H} are nearly orthogonal to each other. Therefore, the ZF receiver can achieve almost maximum channel capacity without precoding at the optimal criteria. When the number of antennas is large, the channel capacity is achieved by the ZF receiver in conjunction with the successive interference cancellation (SIC) of data streams.

IV. PRECODER DESIGN FOR NON-OPTIMAL UCA SYSTEM

Although the optimal design criterion allows us to achieve the maximum capacity, UCA systems that consider longer transmission distances with a limited array size are also preferred from practical implementation perspectives. If the communication distance is longer than the optimal value (or the radii are smaller than the optimal value), the deviation between singular values is considerable as shown in the case of $\beta = 0.5\beta^\circ$ in Table III. Hence precoding is necessary for achieving high data rates.

A. Codebook Based Precoder

Referring to Property 1, the SVD-based capacity achieving the optimal precoding scheme of a UCA system is $\mathbf{V} = \mathbf{T}_t \mathbf{Q}$ with the water-filling power allocation where \mathbf{T}_t is determined by the center-shift angles $\{\theta_{cs}, \phi_{cs}\}$. To implement this optimal precoder, the information of $\{\theta_{cs}, \phi_{cs}\}$ and θ_o is required for precoding and power allocation, respectively; otherwise, full channel-state information is necessary. Because the center-shift angles can be viewed as the directions of arrival (DoAs) when the center of the Tx UCA is regarded as a source point, existing estimation techniques, such as the multiple-signal classification (MUSIC) algorithm can be used to obtain those angles. However, tilting of the Rx UCA induces phase offsets of the center-shift angles (or DoAs), which degrade estimation accuracy (we demonstrate this through computer simulations in the next section).

An alternative approach is to construct a codebook with angular quantizations. We quantize the center-shift angles so that their sine values are uniformly distributed within ranges determined by the angular ranges of the center-shift angles. This is because the phase term of \mathbf{T}_t in (11) is proportional to the sines of θ_{cs} and ϕ_{cs} . Because ϕ_{cs} represents the degree of shift, an angular range of ϕ_{cs} can be narrow in wireless backhaul scenarios in which deviations might be small. For example, when $D = 100$ meters and the Rx UCA moves 10 meters from the z -axis and then $\phi_{cs} = 0.1$ rad (5.73°), the angular range of ϕ_{cs} can be set as $[-0.175 \text{ rad } (-10^\circ), 0.175 \text{ rad } (10^\circ)]$. However, θ_{cs} represents the direction of the center-shift, which ranges from $-\pi$ to π . Thus, its angular range should be $[-\pi/2, \pi/2]$ because we quantize $\sin \theta_{cs}$, and $\sin(\pi - \theta_{cs}) = \sin \theta_{cs}$.

¹In fact, the capacity tends to increase linearly with N_s . This can be seen from the following capacity upper bound, which is valid under a high-SNR regime [20]: $C_{N_s} \leq N_s \log(\frac{P_T}{N_s N_o} \sum_{k=1}^{N_s} \sigma_k^2) = N_s \log \frac{P_T}{N_o}$, where the equality holds due to (17).

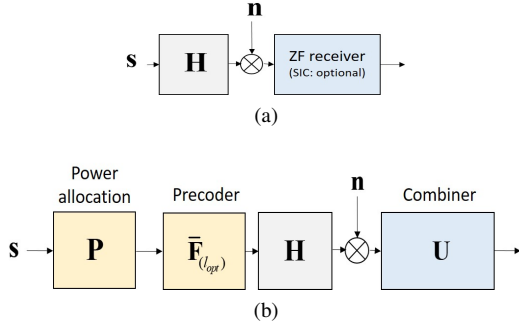


Fig. 7. Proposed transceiver architectures for misaligned UCA systems. (a) At the optimal criterion. (b) When the optimal criterion is not satisfied.

Let the center-shift angles $\{\theta_{cs}, \phi_{cs}\}$ be quantized to 2^{L_1} and 2^{L_2} elements, respectively. Then we have 2^L sets of angles, where $L = L_1 + L_2$. We denote the set of angles as $\bar{\mathcal{A}}_{(l)} = \{\bar{\theta}_{cs(l_1)}, \bar{\phi}_{cs(l_2)}\}$, where $l = 1, \dots, 2^L$ and $\bar{\theta}_{cs(l_1)}$ ($\bar{\phi}_{cs(l_2)}$) is the l_1^{th} (l_2^{th}) quantized angle of θ_{cs} (ϕ_{cs}) among 2^{L_1} (2^{L_2}) elements. The optimal set of angles is determined by a selection algorithm operating at Rx; and the Rx transfers L bits index of the optimal set to the Tx. Let $\bar{\mathbf{T}}_{t(l)}$ denote \mathbf{T}_t obtained by the quantized angles from the set $\bar{\mathcal{A}}_{(l)}$. We consider the maximum achievable rate as a performance metric, and then the receiver can search for the codebook index that solves

$$l_{opt} = \arg \max_{0 \leq l \leq 2^L} \log_2 \det(\mathbf{I}_{N_s} + \mathbf{H} \bar{\mathbf{F}}_{(l)} \mathbf{P} \bar{\mathbf{F}}_{(l)}^H \mathbf{H}^H). \quad (19)$$

Here, \mathbf{P} is a diagonal matrix whose k^{th} diagonal entry is given by p_k/N_o and $\bar{\mathbf{F}}_{(l)} \triangleq \bar{\mathbf{T}}_{t(l)} \mathbf{Q}$. The water-filling power allocations $\{p_k\}$ can be approximated by the following power allocation policy.

B. Approximate Power Allocation

Because of the robustness of singular values against θ_o , the power allocations of the misaligned UCA system can be substituted with the power allocations designed for the aligned UCA system where $\theta_o = 0$. This roughly performed power allocation only requires the information of D at given R_t , R_r , λ , and N_s , without cumbersome estimation of θ_o , but only minor performance degradation appears, which will be demonstrated via computer simulations in Section V.

The proposed transceiver architectures for the optimal and non-optimal UCA systems to achieve the channel capacity without estimating or compensating misalignment angles are illustrated in Fig. 7. The optimally designed UCA systems and the non-optimal UCA systems are complementary to each others. The optimal UCA systems achieve the maximum capacity by the simple ZF receiver at the expense of large UCA radii, whereas the non-optimal UCA systems can fit in a small space but require precoding and suffer from capacity reduction. Two natural questions from an implementation point of view are how far the ZF receiver can support the capacity and when precoding is worthwhile at the fixed UCA radii. To answer these questions, we investigate the performance of the two transceivers through computer simulations.

V. SIMULATION RESULTS

The performance of the proposed transceivers of a misaligned UCA system is examined through computer simulations with the following parameters: the carrier frequency is 75 GHz ($\lambda = 2mm$), SNR=15 dB, and the radii of the Tx/Rx UCAs are assumed to be equal. i.e., $R_t = R_r$, and fixed to the optimal value at the communication distance of 100 meters. All results are obtained by averaging over 100 channel realizations, in which misalignment angles are randomly generated to have a uniform distribution with a zero mean. We assume that the misalignment angles $\{\varphi_x, \varphi_y, \phi_{cs}, \theta_o\}$ are within the interval $[-\frac{10}{180}\pi, \frac{10}{180}\pi]$, except for θ_{cs} which is in the interval $[-\pi, \pi]$.

This section consists of two parts. In the first part, we examine the performance of proposed codebook-based precoder and approximated water-filling power allocation policy. Then, in the second part, we compare the performance of two transceiver systems in Fig. 7 to provide guidelines for transceiver implementation.

A. Performance Evaluation of Proposed Precoding scheme

The performance of the proposed codebook-based precoder is compared with that of its benchmarks: the optimal precoder, the precoder obtained by the MUSIC algorithm, and the identity precoder. The metric for the performance comparison is the maximum achievable rate. For the MUSIC estimation, we assumed that an antenna on the Tx UCA acts as a source point so that the source signal transmitted from the m^{th} Tx antenna is conveyed through the channel corresponding to the m^{th} column vector of \mathbf{H} . Then, the Rx computes the MUSIC algorithm using the array response vector of the UCA [21]. Since the difference between the m^{th} column vector of \mathbf{H} and the array response vector of the UCA mainly comes from tilting, this setting reflects the effects of tilting on the MUSIC estimation.

Fig. 8 shows the maximum achievable rate curves of the proposed precoder and its benchmarks against D when $N_s = 4, 8, 12$ and 16, and the codebook bits of the proposed precoder are given as $(L_1, L_2) = (5, 3)$ bits. The results show that the maximum achievable rates of the proposed precoder coincide with the channel capacity when $N_s = 4$ and 8, but when $N_s = 12$ and 16, there is a small gap between them. Because the performance of the proposed approximated water-filling power allocation is the same as that of the optimal power allocation, the approximation in computing power allocations has little effect on the performance degradation. The gap mainly comes from the quantizations in codebook design. The gap tends to increase with the number of antennas because the greater the deviation between singular values the more sensitive the precoder performance is. Noticeable precoding gains over the identity precoder appear when the communication distance exceeds about 200 meters. When $D = 300$ meters, the proposed precoder provides about 4 bits/sec/Hz gains over the identity precoder when $N_s \geq 12$. When $D = 500$ meters, precoding gains of more than 9% appear with all numbers of antennas. Interestingly, the maximum achievable rate of the precoder obtained by the MUSIC algorithm is lower than that

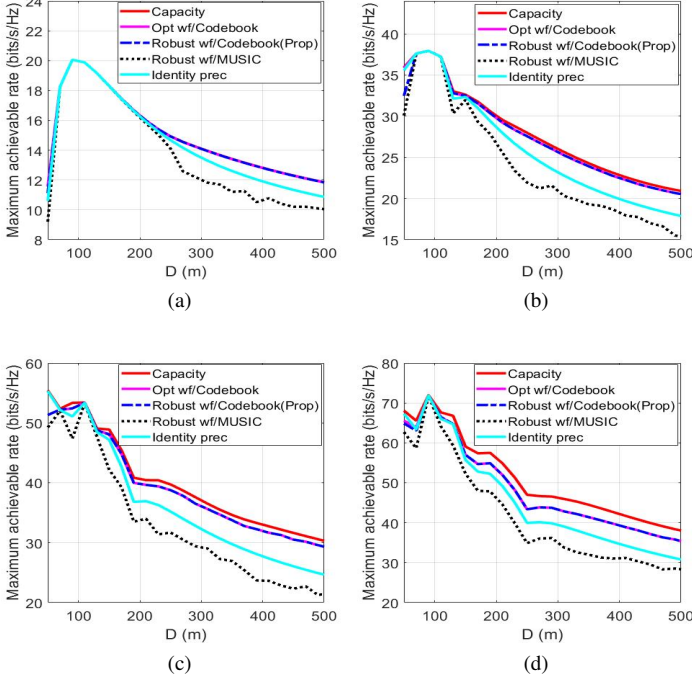


Fig. 8. Maximum achievable rate curves of the proposed precoder and its benchmarks against D . The number of bits of codebook $L = 8$ bits ($L_1 = 5$ bits and $L_2 = 3$ bits). (a) $N_s = 4$. (b) $N_s = 8$. (c) $N_s = 12$. (d) $N_s = 16$.

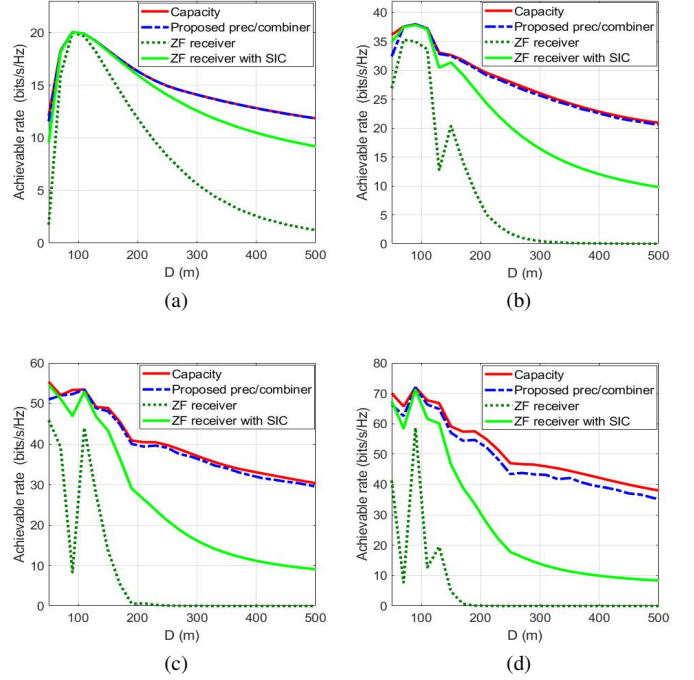


Fig. 10. Achievable rate curves of the proposed transceiver architectures of UCA systems against D . The number of bits of codebook $L = 8$ bits ($L_1 = 5$ bits and $L_2 = 3$ bits). (a) $N_s = 4$. (b) $N_s = 8$. (c) $N_s = 12$. (d) $N_s = 16$.

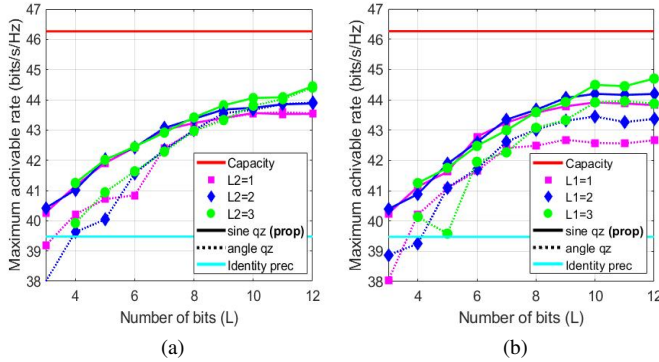


Fig. 9. Maximum achievable rate curves of the proposed precoder against the number of codebook bits L when $N_s = 16$ and $D = 300$ meters. (a) L_2 is fixed. (b) L_1 is fixed.

of the identity precoder. This is because the phase offsets of the center-shift angles (or DoAs) induced by tilting of the Rx UCA result in significant performance degradation, as we discussed at the beginning of Section IV.

Fig. 9 shows the impacts of bit allocations and the quantization method in codebook design when $N_s = 16$ and $D = 300$ meters. We compare the codebook designed by the proposed quantization method in which the angles are quantized to have uniformly distributed sine values, with the codebook designed by linear quantization of the angles, and show that the proposed quantization method outperforms the linear quantization method. We also compare two types of codebook bit-allocation methods: Fig. 9(a) shows the performance of codebooks in which L_2 is fixed to 1, 2, and 3 bits, respectively, and L_1

increases so that more bits are allocated to θ_{cs} , and Fig. 9(b) shows that of the opposite case. Comparing the codebook bit-allocations, the performance of the codebook depends on the total number of codebook bits, not the bit-allocation method. This is because, even though the angular range of θ_{cs} is much larger than that of ϕ_{cs} , θ_m is dominant to determine the term $\sin(\theta_m + \theta_{cs})$ in (11); thus, θ_{cs} has a small effect on the performance compared to its degree of deviation. The maximum achievable rates of the proposed precoder increase linearly with L when $L \leq 8$, but saturate beyond that.

B. Comparison of Proposed Transceiver Architectures

Fig. 10 shows the achievable rate curves of the two proposed transceiver architectures illustrated in Fig. 7 against D when $N_s \in \{4, 8, 12, 16\}$. As expected, precoding gains are minor at the optimal distance (100 meters), and the ZF receiver achieves the channel capacity when $N_s = 4$. When $N_s = 8, 12$, and 16, the ZF receiver achieves the channel capacity with the help of the SIC. The ZF receiver tolerates small deviations of D from its optimal value, but the performance gap between the ZF receiver and the proposed precoder and combiner scheme is considerable when the communication distance exceeds 150 meters. Therefore, we propose the use of the ZF receiver when the deviation of D is within a few meters; otherwise, the proposed precoder/combiner system is recommended.

VI. CONCLUSION

We proposed an optimal design method and transceiver architectures for misaligned UCA systems, which can be implemented without the knowledge of misalignment angles.

We derived a channel model of the misaligned UCA system, and from the derived channel model, it was shown that the singular values of the misaligned UCA system varies with an RPDR value but is robust to other misalignments. Then, we proposed an optimal design method of UCA systems that performs a one-dimensional search of RPDR to maximize the channel capacity. A ZF receiver without precoding was suggested as the optimal transceiver architecture for the optimally designed UCA system. For the non-optimal UCA system, a codebook-based precoder was proposed, in which the codebook is designed by quantization of the center-shift angles and approximated power allocation. Simulation results showed that the ZF receiver achieves the channel capacity at the optimal design criteria, and when the optimal design criteria cannot be met, the proposed precoder can achieve the capacity with low feedback overhead. In future works, it would be interesting to extend this research to fast-moving scenarios, such as UAV backhaul systems or high-speed railway backhaul systems, which also have potential to leverage the robustness of misalignments of UCA-based MIMO systems over LoS channel environments.

APPENDIX A PROOF OF LEMMA 3

The distance $d(n, m)$ can be written as (20) where the equality (a) follows from $\cos^2 x = \frac{\cos(2x)+1}{2}$ and the equality (b) comes from the fact that $(b_{11}^2 + b_{12}^2 + b_{21}^2 + b_{22}^2 + b_{31}^2 + b_{32}^2) = 2$ and b_{ij} is the $(i, j)^{th}$ element of $R_{\theta_{cs}}^{xy} R_{\varphi_x}^{xz} R_{\varphi_y}^{yz}$ given by (21). Using $\sqrt{b_{i1}^2 + b_{i2}^2} \cos(\theta_n - \theta_o) = b_{i1} \cos(\theta_n + \theta_o) + b_{i2} \sin(\theta_n + \theta_o)$, the term $\{1\}$ in (20) becomes (22) where the last equality follows from $\cos x = 1 - 2 \sin^2 \frac{x}{2}$. From (22), $d(n, m)$ in (20) is rewritten as (23).

APPENDIX B PROOFS OF PROPERTIES 2(a)–(e)

A. Proof of property 2(a)

Let us abbreviate $\sigma_k(\beta, \theta_o)$ to σ_k . Referring to (17), σ_k is given by

$$\begin{aligned} \sigma_k &= \left| \sum_{i=0}^{N_s-1} e^{-j\left(\frac{2\pi}{N_s}i(k-1) - \beta \cos\left(\frac{2\pi}{N_s}i + \theta_o\right)\right)} \right| \\ &= \left| \sum_{i=0}^{\frac{N_s}{2}-1} e^{-j\left(\frac{2\pi}{N_s}i(k-1) - \beta \cos\left(\frac{2\pi}{N_s}i + \theta_o\right)\right)} \right. \\ &\quad \left. + \sum_{i=\frac{N_s}{2}}^{N_s-1} e^{-j\left(\frac{2\pi}{N_s}i(k-1) - \beta \cos\left(\frac{2\pi}{N_s}i + \theta_o\right)\right)} \right| \\ &= \left| \sum_{i=0}^{\frac{N_s}{2}-1} e^{-j\left(\frac{2\pi}{N_s}i(k-1)\right)} \cdot e^{+j\left(\beta \cos\left(\frac{2\pi}{N_s}i + \theta_o\right)\right)} \right. \\ &\quad \left. + \sum_{i=0}^{\frac{N_s}{2}-1} e^{-j\left(\frac{2\pi}{N_s}i(k-1) + \pi(k-1)\right)} \cdot e^{-j\left(\beta \cos\left(\frac{2\pi}{N_s}i + \theta_o\right)\right)} \right| \\ &= \left| \sum_{i=0}^{\frac{N_s}{2}-1} e^{-j\left(\frac{2\pi}{N_s}i(k-1)\right)} \right. \\ &\quad \left. \times \left\{ e^{+j\left(\beta \cos\left(\frac{2\pi}{N_s}i + \theta_o\right)\right)} + (-1)^{k-1} e^{-j\left(\beta \cos\left(\frac{2\pi}{N_s}i + \theta_o\right)\right)} \right\} \right|. \end{aligned} \quad (24)$$

Let $k' = N_s + 2 - k$, and $\sigma_{k'}$ is given by

$$\begin{aligned} \sigma_{k'} &= \left| \sum_{i=0}^{N_s-1} e^{-j\left(\frac{2\pi}{N_s}i(k'-1) - \beta \cos\left(\frac{2\pi}{N_s}i + \theta_o\right)\right)} \right| \\ &= \left| \sum_{i=0}^{N_s-1} e^{+j\left(\frac{2\pi}{N_s}i(k-1) + \beta \cos\left(\frac{2\pi}{N_s}i + \theta_o\right)\right)} \right| \\ &= \left| \sum_{i=0}^{\frac{N_s}{2}-1} e^{+j\left(\frac{2\pi}{N_s}i(k-1) + \beta \cos\left(\frac{2\pi}{N_s}i + \theta_o\right)\right)} \right. \\ &\quad \left. + \sum_{i=\frac{N_s}{2}}^{N_s-1} e^{+j\left(\frac{2\pi}{N_s}i(k-1) + \beta \cos\left(\frac{2\pi}{N_s}i + \theta_o\right)\right)} \right| \\ &= \left| \sum_{i=0}^{\frac{N_s}{2}-1} e^{+j\left(\frac{2\pi}{N_s}i(k-1) + \beta \cos\left(\frac{2\pi}{N_s}i + \theta_o\right)\right)} \right. \\ &\quad \left. + \sum_{i=0}^{\frac{N_s}{2}-1} e^{+j\left(\frac{2\pi}{N_s}i(k-1) + \pi(k-1)\right)} e^{-j\left(\beta \cos\left(\frac{2\pi}{N_s}i + \theta_o\right)\right)} \right| \\ &= \left| \sum_{i=0}^{\frac{N_s}{2}-1} e^{+j\left(\frac{2\pi}{N_s}i(k-1)\right)} \right. \\ &\quad \left. \times \left\{ e^{+j\left(\beta \cos\left(\frac{2\pi}{N_s}i + \theta_o\right)\right)} + (-1)^{k-1} e^{-j\left(\beta \cos\left(\frac{2\pi}{N_s}i + \theta_o\right)\right)} \right\} \right|. \end{aligned} \quad (25)$$

To show that $\sigma_k = \sigma_{k'}$, we divide the proof into two cases for even and odd values of k . When k is odd, σ_k is given by

$$\begin{aligned} \sigma_k &= 2 \left| \sum_{i=0}^{\frac{N_s}{2}-1} e^{-j\left(\frac{2\pi}{N_s}i(k-1)\right)} \cos\left(\beta \cos\left(\frac{2\pi}{N_s}i + \theta_o\right)\right) \right| \\ &= \left| \sum_{i=0}^{\frac{N_s}{2}-1} e^{-j\left(\frac{2\pi}{N_s}i(k-1)\right)} \cos\left(\beta \cos\left(\frac{2\pi}{N_s}i + \theta_o\right)\right) \right. \\ &\quad \left. + \sum_{i=\frac{N_s}{2}}^{N_s-1} e^{-j\left(\frac{2\pi}{N_s}(i - \frac{N_s}{2})(k-1)\right)} \cos\left(\beta \cos\left(\frac{2\pi}{N_s}(i - \frac{N_s}{2}) + \theta_o\right)\right) \right| \\ &= \left| \sum_{i=0}^{\frac{N_s}{2}-1} e^{-j\left(\frac{2\pi}{N_s}i(k-1)\right)} \cos\left(\beta \cos\left(\frac{2\pi}{N_s}i + \theta_o\right)\right) \right| \\ &= \left[\left\{ \sum_{i=0}^{\frac{N_s}{2}-1} \cos\left(\frac{2\pi}{N_s}i(k-1)\right) \cos\left(\beta \cos\left(\frac{2\pi}{N_s}i + \theta_o\right)\right) \right\}^2 \right. \\ &\quad \left. + \left\{ \sum_{i=0}^{\frac{N_s}{2}-1} \sin\left(\frac{2\pi}{N_s}i(k-1)\right) \cos\left(\beta \cos\left(\frac{2\pi}{N_s}i + \theta_o\right)\right) \right\}^2 \right]^{\frac{1}{2}}. \end{aligned} \quad (26)$$

Similarly, $\sigma_{k'}$ is given by

$$\begin{aligned} \sigma_{k'} &= 2 \left| \sum_{i=0}^{\frac{N_s}{2}-1} e^{+j\left(\frac{2\pi}{N_s}i(k-1)\right)} \cos\left(\beta \cos\left(\frac{2\pi}{N_s}i + \theta_o\right)\right) \right| \\ &= \left[\left\{ \sum_{i=0}^{\frac{N_s}{2}-1} \cos\left(\frac{2\pi}{N_s}i(k-1)\right) \cos\left(\beta \cos\left(\frac{2\pi}{N_s}i + \theta_o\right)\right) \right\}^2 \right. \\ &\quad \left. + \left\{ \sum_{i=0}^{\frac{N_s}{2}-1} \sin\left(\frac{2\pi}{N_s}i(k-1)\right) \cos\left(\beta \cos\left(\frac{2\pi}{N_s}i + \theta_o\right)\right) \right\}^2 \right]^{\frac{1}{2}} \\ &= \sigma_k. \end{aligned} \quad (27)$$

$$\begin{aligned}
d(n, m) &= \{(R_t \cos \theta'_m - R_1 \cos(\theta_n - \alpha_1))^2 + (R_t \sin \theta'_m - R_2 \cos(\theta_n - \alpha_2) - D \sin \phi_{cs})^2 + (R_3 \cos(\theta_n - \alpha_3) + D \cos \phi_{cs})^2\}^{\frac{1}{2}} \\
&= [R_t^2 + R_r^2 \{(b_{11}^2 + b_{12}^2) \cos^2(\theta_n - \alpha_1) + (b_{21}^2 + b_{22}^2) \cos^2(\theta_n - \alpha_2) + (b_{31}^2 + b_{32}^2) \cos(\theta_n - \alpha_3)\} \\
&\quad - 2R_t R_r \{\sqrt{b_{11}^2 + b_{12}^2} \cos \theta'_m \cos(\theta_n - \alpha_1) + \sqrt{b_{21}^2 + b_{22}^2} \sin \theta'_m \cos(\theta_n - \alpha_2)\} + 2D \{R_r \sqrt{b_{21}^2 + b_{22}^2} \cos(\theta_n - \alpha_2) \sin \phi_{cs} \\
&\quad + R_r \sqrt{b_{31}^2 + b_{32}^2} \cos(\theta_n - \alpha_3) \cos \phi_{cs} - R_t \sin \theta'_m \sin \phi_{cs} + D^2\}]^{\frac{1}{2}} \\
&\stackrel{(a)}{=} [R_t^2 + R_r^2 \{\frac{1}{2}(b_{11}^2 + b_{12}^2 + b_{21}^2 + b_{22}^2 + b_{31}^2 + b_{32}^2) + \frac{1}{2}(\cos 2(\theta_n - \alpha_1) + \cos 2(\theta_n - \alpha_2) + \cos 2(\theta_n - \alpha_3))\} \\
&\quad - 2R_t R_r \{\sqrt{b_{11}^2 + b_{12}^2} \cos \theta'_m \cos(\theta_n - \alpha_1) + \sqrt{b_{21}^2 + b_{22}^2} \sin \theta'_m \cos(\theta_n - \alpha_2)\} + 2D \{R_r \sqrt{b_{21}^2 + b_{22}^2} \cos(\theta_n - \alpha_2) \sin \phi_{cs} \\
&\quad + R_r \sqrt{b_{31}^2 + b_{32}^2} \cos(\theta_n - \alpha_3) \cos \phi_{cs} - R_t \sin \theta'_m \sin \phi_{cs} + D^2\}]^{\frac{1}{2}} \\
&\stackrel{(b)}{=} [R_t^2 + \frac{R_r^2}{2} \{\cos 2(\theta_n - \alpha_1) + \cos 2(\theta_n - \alpha_2) + \cos 2(\theta_n - \alpha_3)\} \\
&\quad - 2R_t R_r \underbrace{\{\sqrt{b_{11}^2 + b_{12}^2} \cos \theta'_m \cos(\theta_n - \alpha_1) + \sqrt{b_{21}^2 + b_{22}^2} \sin \theta'_m \cos(\theta_n - \alpha_2)\}}_{\{1\}} \\
&\quad + 2D \{R_r \sqrt{b_{21}^2 + b_{22}^2} \cos(\theta_n - \alpha_2) \sin \phi_{cs} + R_r \sqrt{b_{31}^2 + b_{32}^2} \cos(\theta_n - \alpha_3) \cos \phi_{cs} - R_t \sin \theta'_m \sin \phi_{cs} + D^2\}]^{\frac{1}{2}}
\end{aligned} \tag{20}$$

$$R_{\theta_{cs}}^{xy} R_{\varphi_x}^{xz} R_{\varphi_y}^{yz} = \begin{bmatrix} \cos \theta_{cs} \cos \varphi_x & -\cos \theta_{cs} \sin \varphi_x \sin \varphi_y - \sin \theta_{cs} \cos \varphi_y & -\cos \theta_{cs} \sin \varphi_x \cos \varphi_y + \sin \theta_{cs} \sin \varphi_y \\ \sin \theta_{cs} \cos \varphi_x & -\sin \theta_{cs} \sin \varphi_x \sin \varphi_y + \cos \theta_{cs} \cos \varphi_y & -\sin \theta_{cs} \sin \varphi_x \cos \varphi_y - \cos \theta_{cs} \sin \varphi_y \\ \sin \varphi_x & \cos \varphi_x \sin \varphi_y & \cos \varphi_x \cos \varphi_y \end{bmatrix} \tag{21}$$

$$\begin{aligned}
\{1\} &= -2R_t R_r \{b_{11} \cos \theta'_m \cos(\theta_n + \theta_o) + b_{12} \cos \theta'_m \sin(\theta_n + \theta_o) + b_{21} \sin \theta'_m \cos(\theta_n + \theta_o) + b_{22} \sin \theta'_m \sin(\theta_n + \theta_o)\} \\
&= -2R_t R_r \{\cos \theta_{cs} \cos \varphi_x \cos \theta'_m \cos(\theta_n + \theta_o) - \cos \theta_{cs} \sin \varphi_x \sin \varphi_y \cos \theta'_m \sin(\theta_n + \theta_o) \\
&\quad - \sin \theta_{cs} \cos \varphi_y \cos \theta'_m \sin(\theta_n + \theta_o) + \sin \theta_{cs} \cos \varphi_x \sin \theta'_m \cos(\theta_n + \theta_o) \\
&\quad - \sin \theta_{cs} \sin \varphi_x \sin \varphi_y \sin \theta'_m \sin(\theta_n + \theta_o) + \cos \theta_{cs} \cos \varphi_y \sin \theta'_m \sin(\theta_n + \theta_o)\} \\
&= -2R_t R_r \{\cos \varphi_x \cos(\theta'_m - \theta_{cs}) \cos(\theta_n + \theta_o) - \sin \varphi_x \sin \varphi_y \cos(\theta'_m - \theta_{cs}) \sin(\theta_n + \theta_o) + \cos \varphi_y \sin(\theta'_m - \theta_{cs}) \sin(\theta_n + \theta_o)\} \\
&= -2R_t R_r \{\cos(\theta_n - \theta'_m + \theta_o + \theta_{cs}) - 2 \sin^2 \frac{\varphi_x}{2} \cos(\theta'_m - \theta_{cs}) \cos(\theta_n + \theta_o) - 2 \sin^2 \frac{\varphi_y}{2} \sin(\theta'_m - \theta_{cs}) \sin(\theta_n + \theta_o) \\
&\quad - \sin \varphi_x \sin \varphi_y \cos(\theta'_m - \theta_{cs}) \sin(\theta_n + \theta_o)\}.
\end{aligned} \tag{22}$$

$$\begin{aligned}
d(n, m) &= [D^2 + R_t^2 + R_r^2 - 2R_t R_r \cos(\theta_n - \theta'_m + \theta_o + \theta_{cs}) + \frac{R_r^2}{2} \{\cos 2(\theta_n - \alpha_1) + \cos 2(\theta_n - \alpha_2) + \cos 2(\theta_n - \alpha_3)\} \\
&\quad + 2R_t R_r \{2 \sin^2 \frac{\varphi_x}{2} \cos(\theta'_m - \theta_{cs}) \cos(\theta_n + \theta_o) + 2 \sin^2 \frac{\varphi_y}{2} \sin(\theta'_m - \theta_{cs}) \sin(\theta_n + \theta_o) \\
&\quad + \sin \varphi_x \sin \varphi_y \cos(\theta'_m - \theta_{cs}) \sin(\theta_n + \theta_o)\} + 2D \{R_2 \cos(\theta_n - \alpha_2) \sin \phi_{cs} + R_3 \cos(\theta_n - \alpha_3) \cos \phi_{cs}\} - R_t \sin \theta'_m \sin \phi_{cs}]^{\frac{1}{2}} \\
&= D \left[1 + \frac{R_t^2 + R_r^2}{D^2} - \frac{2R_t R_r}{D^2} \cos(\theta_n - \theta_m + \theta_o) + \frac{R_r^2}{2D^2} \{(\cos 2(\theta_n - \alpha_1) + \cos 2(\theta_n - \alpha_2) + \cos 2(\theta_n - \alpha_3))\} \right. \\
&\quad + \frac{4R_t R_r}{D^2} \left\{ \sin^2 \frac{\varphi_x}{2} \cos \theta_m \cos(\theta_n + \theta_o) + \sin^2 \frac{\varphi_y}{2} \sin \theta_m \sin(\theta_n + \theta_o) + \frac{1}{2} \sin \varphi_x \sin \varphi_y \cos \theta_m \sin(\theta_n + \theta_o) \right\} \\
&\quad \left. + \frac{2}{D} \{R_2 \cos(\theta_n - \alpha_2) \sin \phi_{cs} + R_3 \cos(\theta_n - \alpha_3) \cos \phi_{cs} - R_t \sin \theta'_m \sin \phi_{cs}\} \right]^{\frac{1}{2}} \\
&= D \{1 + f(R_t, R_r, D, \theta_m, \theta_n, \theta_o, \theta_{cs}, \varphi_x, \varphi_y, \phi_{cs})\}^{\frac{1}{2}}
\end{aligned} \tag{23}$$

When k is even, we have

and

$$\begin{aligned}
\sigma_k &= 2 \left| j \sum_{i=0}^{\frac{N_s}{2}-1} e^{-j \left(\frac{2\pi}{N_s} i(k-1) \right)} \sin \left(\beta \cos \left(\frac{2\pi}{N_s} i + \theta_o \right) \right) \right| \\
&= \left| j \sum_{i=0}^{\frac{N_s}{2}-1} e^{-j \left(\frac{2\pi}{N_s} i(k-1) \right)} \sin \left(\beta \cos \left(\frac{2\pi}{N_s} i + \theta_o \right) \right) \right|
\end{aligned} \tag{28}$$

$$\begin{aligned}
\sigma_{k'} &= 2 \left| j \sum_{i=0}^{\frac{N_s}{2}-1} e^{+j \left(\frac{2\pi}{N_s} i(k-1) \right)} \sin \left(\beta \cos \left(\frac{2\pi}{N_s} i + \theta_o \right) \right) \right| \\
&= \left| j \sum_{i=0}^{\frac{N_s}{2}-1} e^{+j \left(\frac{2\pi}{N_s} i(k-1) \right)} \sin \left(\beta \cos \left(\frac{2\pi}{N_s} i + \theta_o \right) \right) \right|,
\end{aligned} \tag{29}$$

and the remaining proof is handled similarly to the odd case.

B. Proof of property 2(b)

Let us consider odd and even values of k separately. Referring to (26), when k is odd, σ_k is upper bounded as

$$\begin{aligned}\sigma_k &= \left| \sum_{i=0}^{N_s-1} e^{-j\left(\frac{2\pi}{N_s}i(k-1)\right)} \cos\left(\beta \cos\left(\frac{2\pi}{N_s}i + \theta_o\right)\right) \right| \\ &\leq \sum_{i=0}^{N_s-1} \left| e^{-j\left(\frac{2\pi}{N_s}i(k-1)\right)} \cos\left(\beta \cos\left(\frac{2\pi}{N_s}i + \theta_o\right)\right) \right| \\ &= \sum_{i=0}^{N_s-1} \left| \cos\left(\beta \cos\left(\frac{2\pi}{N_s}i + \theta_o\right)\right) \right|,\end{aligned}\quad (30)$$

where the second inequality comes from the triangle inequality. What we want to find is a range of β such that

$$\sum_{i=0}^{N_s-1} \left| \cos\left(\beta \cos\left(\frac{2\pi}{N_s}i + \theta_o\right)\right) \right| \leq \sum_{i=0}^{N_s-1} \cos\left(\beta \cos\left(\frac{2\pi}{N_s}i + \theta_o\right)\right), \quad (31)$$

where the upper bound is equal to σ_1 . Because of the triangle inequality, (31) is true only when the equality holds. Thus, the range of β is obtained as $0 \leq \beta \leq \pi/2$ where $\cos\left(\beta \cos\left(\frac{2\pi}{N_s}i + \theta_o\right)\right) \geq 0$ for all i .² Similarly, σ_k of the even value k is given by

$$\begin{aligned}\sigma_k &= 2 \left| j \sum_{i=0}^{\frac{N_s}{2}-1} e^{-j\left(\frac{2\pi}{N_s}i(k-1)\right)} \sin\left(\beta \cos\left(\frac{2\pi}{N_s}i + \theta_o\right)\right) \right| \\ &= \left| \sum_{i=0}^{N_s-1} j e^{-j\left(\frac{2\pi}{N_s}i(k-1)\right)} \sin\left(\beta \cos\left(\frac{2\pi}{N_s}i + \theta_o\right)\right) \right| \\ &\leq \sum_{i=0}^{N_s-1} \left| j e^{-j\left(\frac{2\pi}{N_s}i(k-1)\right)} \sin\left(\beta \cos\left(\frac{2\pi}{N_s}i + \theta_o\right)\right) \right| \\ &= \sum_{i=0}^{N_s-1} \left| \sin\left(\beta \cos\left(\frac{2\pi}{N_s}i + \theta_o\right)\right) \right|.\end{aligned}\quad (32)$$

To find the range of β such that

$$\sum_{i=0}^{N_s-1} \left| \sin\left(\beta \cos\left(\frac{2\pi}{N_s}i + \theta_o\right)\right) \right| \leq \sum_{i=0}^{N_s-1} \cos\left(\beta \cos\left(\frac{2\pi}{N_s}i + \theta_o\right)\right), \quad \beta = 0, \quad (33)$$

let $\theta_i \triangleq \beta \cos\left(\frac{2\pi}{N_s}i + \theta_o\right)$. To compare with the range of β found in the case of odd value k , we consider $\beta \in [0, \pi/2]$. Then, (33) is rewritten as

$$\sum_{i=0}^{N_s-1} |\sin \theta_i| \leq \sum_{i=0}^{N_s-1} |\cos \theta_i|, \quad (34)$$

where $-\pi/2 \leq \theta_i \leq \pi/2$ and $\cos \theta_i \geq 0$. When $0 \leq \beta \leq \pi/4$, (34) is always true because $-\pi/4 \leq \theta_i \leq \pi/4$; thus, $|\sin \theta_i| \leq \cos \theta_i$ for all θ_i . When $\pi/4 \leq \beta \leq \pi/2$, $-\pi/2 \leq \theta_i \leq \pi/2$, let $\theta_{i,1} \in \{\theta_i | -\pi/2 < \frac{2\pi}{N_s}i + \theta_o \leq \pi/2\}$ and $\theta_{i,2} \in \{\theta_i | -\pi < \frac{2\pi}{N_s}i + \theta_o \leq -\pi/2 \text{ or } \pi/2 < \frac{2\pi}{N_s}i + \theta_o \leq \pi\}$, respectively, and the numbers of $\theta_{i,1}$ and $\theta_{i,2}$ are $N_s/2$. Because $|\sin \theta_i|$ is concave in each ranges, we have $\mathbb{E}(|\sin \theta_{i,1}|) + \mathbb{E}(|\sin \theta_{i,2}|) \leq \sin \mathbb{E}(|\theta_{i,1}|) +$

$\sin \mathbb{E}(|\theta_{i,2}|)$. Furthermore, because $0 \leq \mathbb{E}(|\theta_{i,1}|), \mathbb{E}(|\theta_{i,2}|) \leq \pi/2$, we have $\sin \mathbb{E}(|\theta_{i,1}|) + \sin \mathbb{E}(|\theta_{i,2}|) \leq 2 \sin \mathbb{E}(|\theta_i|)$. Thus,

$$\begin{aligned}\sum_{i=0}^{N_s-1} |\sin \theta_i| &\leq \frac{N_s}{2} (\sin \mathbb{E}(|\theta_{i,1}|) + \sin \mathbb{E}(|\theta_{i,2}|)) \\ &\leq N_s \sin \mathbb{E}(|\theta_i|).\end{aligned}\quad (35)$$

Similarly, $\sum_{i=0}^{N_s-1} |\cos \theta_i| \leq N_s \cos \mathbb{E}(|\theta_i|)$. Using this, the condition (34) can be rewritten as

$$\sin \mathbb{E}(|\theta_i|) \leq \cos \mathbb{E}(|\theta_i|). \quad (36)$$

To hold (36), $0 \leq \mathbb{E}(|\theta_i|) \leq \frac{\pi}{4}$ and the range of β is obtained as $\pi/4 \leq \beta \leq \frac{\pi N_s}{4 \sum_{i=0}^{N_s-1} |\cos(\frac{2\pi}{N_s}i + \theta_o)|}$. Combining all results, the objective range of β is given by

$$0 \leq \beta \leq \frac{\pi N_s}{4 \sum_{i=0}^{N_s-1} |\cos(\frac{2\pi}{N_s}i + \theta_o)|}. \quad (37)$$

C. Proof of property 2(c)

Let us assume that θ_o is fixed at some value. Then, $\sigma_k(\beta, \theta_o)$ can be written as $\sigma_k(\beta)$. Because $\sigma_k(\beta)$ is a composition function of a sum of continuous sinusoidal functions and an absolute value function which are continuous functions, it is continuous. Therefore, if $\beta \rightarrow 0$ then $\sigma_k(\beta) \rightarrow \sigma_k(0)$. When $\beta = 0$, we have

$$\sigma_k(0) = \left| \sum_{i=0}^{N_s-1} e^{-j\left\{\frac{2\pi}{N_s}i(k-1)\right\}} \right| \quad (38)$$

and it can be easily seen that $\sigma_k(0) = N_s$ when $k = 1$. Otherwise, the sum in (38) is a finite geometric series which is given by

$$\begin{aligned}\sigma_k(0) &= \left| \frac{1 - [e^{-j2\pi(k-1)/N_s}]^{N_s}}{1 - e^{-j2\pi(k-1)/N_s}} \right| \\ &= \left| \frac{1 - e^{-j2\pi(k-1)}}{1 - e^{-j2\pi(k-1)/N_s}} \right|.\end{aligned}\quad (39)$$

Therefore, $\sigma_k(0) = 0$ for $k = 2, \dots, N_s$.

²What we have interest is the range of β starting from 0 to some value that we have $\sigma_k \leq \sigma_1$ for all $k \in \{2, \dots, N_s\}$. Therefore, we ignore other valid ranges of β which are over than $[0, \pi/2]$.

D. Proof of property 2(d)

Let $i = N_s - 1 - i'$ where $i, i' \in \{0, \dots, N_s - 1\}$. Referring to (26), when k is odd, $\sigma_k(\beta, -\theta_o)$ is given by

$$\begin{aligned}
 \sigma_k(\beta, -\theta_o) &= \left| \sum_{i=0}^{N_s-1} e^{-j\left(\frac{2\pi}{N_s}i(k-1)\right)} \cos\left(\beta \cos\left(\frac{2\pi}{N_s}i - \theta_o\right)\right) \right| \\
 &= \left| \sum_{i'=0}^{N_s-1} e^{-j\left(\frac{2\pi}{N_s}(N_s-1-i')(k-1)\right)} \right. \\
 &\quad \times \left. \cos\left(\beta \cos\left(\frac{2\pi}{N_s}(N_s-1-i') - \theta_o\right)\right) \right| \\
 &= \left| \sum_{i'=0}^{N_s-1} e^{+j\left(\frac{2\pi}{N_s}(i'+1)(k-1)\right)} \cos\left(\beta \cos\left(\frac{2\pi}{N_s}(i'+1) + \theta_o\right)\right) \right| \\
 &\stackrel{(a)}{=} \left| \sum_{i'=0}^{N_s-1} e^{+j\left(\frac{2\pi}{N_s}i'(k-1)\right)} \cos\left(\beta \cos\left(\frac{2\pi}{N_s}i' + \theta_o\right)\right) \right| \\
 &= \left| \sum_{i'=0}^{N_s-1} \cos\left(\frac{2\pi}{N_s}i'(k-1)\right) \cos\left(\beta \cos\left(\frac{2\pi}{N_s}i' + \theta_o\right)\right) \right. \\
 &\quad \left. + j \sum_{i'=0}^{N_s-1} \sin\left(\frac{2\pi}{N_s}i'(k-1)\right) \cos\left(\beta \cos\left(\frac{2\pi}{N_s}i' + \theta_o\right)\right) \right| \\
 &= \left[\left\{ \sum_{i'=0}^{N_s-1} \cos\left(\frac{2\pi}{N_s}i'(k-1)\right) \cos\left(\beta \cos\left(\frac{2\pi}{N_s}i' + \theta_o\right)\right) \right\}^2 \right. \\
 &\quad \left. + \left\{ \sum_{i'=0}^{N_s-1} \sin\left(\frac{2\pi}{N_s}i'(k-1)\right) \cos\left(\beta \cos\left(\frac{2\pi}{N_s}i' + \theta_o\right)\right) \right\}^2 \right]^{\frac{1}{2}} \\
 &= \sigma_k(\beta, \theta_o)
 \end{aligned} \tag{40}$$

where the equality (a) comes from the fact that

$$\begin{aligned}
 &e^{-j\left(\frac{2\pi}{N_s}(N_s)(k-1)\right)} \cos\left(\beta \cos\left(\frac{2\pi}{N_s}(N_s) - \theta_o\right)\right) \\
 &= e^{-j\left(\frac{2\pi}{N_s}(0)(k-1)\right)} \cos\left(\beta \cos\left(\frac{2\pi}{N_s}(0) - \theta_o\right)\right).
 \end{aligned}$$

Similarly, when k is even, we get

$$\begin{aligned}
 \sigma_k(\beta, -\theta_o) &= \left| j \sum_{i'=0}^{N_s-1} e^{+j\left(\frac{2\pi}{N_s}i'(k-1)\right)} \sin\left(\beta \cos\left(\frac{2\pi}{N_s}i' + \theta_o\right)\right) \right| \\
 &= \left| j \sum_{i'=0}^{N_s-1} \cos\left(\frac{2\pi}{N_s}i'(k-1)\right) \sin\left(\beta \cos\left(\frac{2\pi}{N_s}i' + \theta_o\right)\right) \right. \\
 &\quad \left. - \sum_{i'=0}^{N_s-1} \sin\left(\frac{2\pi}{N_s}i'(k-1)\right) \sin\left(\beta \cos\left(\frac{2\pi}{N_s}i' + \theta_o\right)\right) \right| \\
 &= \left[\left\{ \sum_{i'=0}^{N_s-1} \cos\left(\frac{2\pi}{N_s}i'(k-1)\right) \sin\left(\beta \cos\left(\frac{2\pi}{N_s}i' + \theta_o\right)\right) \right\}^2 \right. \\
 &\quad \left. + \left\{ \sum_{i'=0}^{N_s-1} \sin\left(\frac{2\pi}{N_s}i'(k-1)\right) \sin\left(\beta \cos\left(\frac{2\pi}{N_s}i' + \theta_o\right)\right) \right\}^2 \right]^{\frac{1}{2}} \\
 &= \sigma_k(\beta, \theta_o).
 \end{aligned} \tag{41}$$

E. Proof of property 2(e)

When $k = N_s/2 + 1$, $\sigma_k(\beta, \theta_o)$ is decomposed into odd and even values of i as

$$\begin{aligned}
 \sigma_{N_s/2+1}(\beta, \theta_o) &= \left| \sum_{i=0}^{N_s-1} e^{-j\pi i} e^{+j\left(\beta \cos\left(\frac{2\pi}{N_s}i + \theta_o\right)\right)} \right| \\
 &= \left| \sum_{i'=0}^{N_s/2-1} \underbrace{e^{+j\left(\beta \cos\left(\frac{2\pi}{N_s}(2i') + \theta_o\right)\right)}}_{\text{even } i} \right. \\
 &\quad \left. - \underbrace{e^{+j\left(\beta \cos\left(\frac{2\pi}{N_s}(2i'+1) + \theta_o\right)\right)}}_{\text{odd } i} \right|.
 \end{aligned} \tag{42}$$

Let $i' = \frac{N_s}{2} - 1 - i''$, then the term of odd value i in (42) can be written as

$$\begin{aligned}
 \cos\left(\frac{2\pi}{N_s}(2i'+1) + \theta_o\right) &= \cos\left(\frac{2\pi}{N_s}\left(2\left(\frac{N_s}{2} - 1 - i''\right) + 1\right) + \theta_o\right) \\
 &= \cos\left(2\pi - \frac{2\pi}{N_s}(2i'' + 1) + \theta_o\right) \\
 &= \cos\left(\frac{2\pi}{N_s}(2i'' + 1) - \theta_o\right).
 \end{aligned} \tag{43}$$

Using this, (42) can be rewritten as

$$\begin{aligned}
 \sigma_{N_s/2+1}(\beta, \theta_o) &= \left| \sum_{i'=0}^{N_s/2-1} e^{+j\left(\beta \cos\left(\frac{2\pi}{N_s}(2i') + \theta_o\right)\right)} \right. \\
 &\quad \left. - \sum_{i''=0}^{N_s/2-1} e^{+j\left(\beta \cos\left(\frac{2\pi}{N_s}(2i''+1) - \theta_o\right)\right)} \right|.
 \end{aligned} \tag{44}$$

Therefore, when $\theta_o = \pi/N_s$,

$$\begin{aligned}
 \sigma_{N_s/2+1}(\beta, \pi/N_s) &= \left| \sum_{i'=0}^{N_s/2-1} e^{+j\left(\beta \cos\left(\frac{2\pi}{N_s}(2i') + \frac{\pi}{N_s}\right)\right)} \right. \\
 &\quad \left. - \sum_{i''=0}^{N_s/2-1} e^{+j\left(\beta \cos\left(\frac{2\pi}{N_s}(2i''+1) + \frac{\pi}{N_s}\right)\right)} \right| \\
 &= 0
 \end{aligned} \tag{45}$$

and the same result can be achieved when $\theta_o = -\pi/N_s$ because of the property 2(d).

REFERENCES

- [1] P. Wang, Y. Li, X. Yuan, L. Song, and B. Vucetic, "Tens of gigabits wireless communications over E-band LoS MIMO channels with uniform linear antenna arrays," *IEEE Trans. Wireless Commun.*, vol. 13, no. 7, pp. 3791-3805, Jul. 2014.
- [2] Xiaohang Song, Wolfgang Rave, Nithin Babu, Sudhan Majhi and Gerhard Fettweis, "Two-level spatial multiplexing using hybrid beamforming for millimeter-wave backhaul," *IEEE Trans. Wireless Commun.*, vol. 17, no. 7, pp. 4830-4844, July. 2018.
- [3] Eric Torkildson, Upamanyu Madhow, and Mark Rodwell, "Indoor millimeter wave MIMO: feasibility and performance," *IEEE Trans. Wireless Commun.*, vol. 10, no. 12, pp. 4150-4160, Dec. 2011.
- [4] Xiaohang Song and Gerhard Fettweis, "On spatial multiplexing of strong line-of-sight MIMO with 3D antenna arrangements," *IEEE Commun. Lett.*, vol. 4, no. 4, pp. 393-396, Aug. 2015.
- [5] F. Bohagen, P. Orten, and G. Oien, "Design of optimal high-rank line-of-sight MIMO channels," *IEEE Trans. Wireless Commun.*, vol. 6, no. 4, pp. 1420-1425, Apr. 2007.
- [6] I. Sarris and A. Nix, "Design and performance assessment of high-capacity MIMO architectures in the presence of a line-of-sight component," *IEEE Trans. Veh. Technol.*, vol. 56, no. 4, pp. 2194-2202, Jul. 2007.

- [7] Lakshmi Natarajan, Yi Hong, Senior Member, IEEE, and Emanuele Viterbo, "Line-of-sight $2 \times nr$ MIMO with random antenna orientations," *IEEE Trans. Veh. Technol.*, vol. 66, no. 6, pp. 5134-5147, Jun. 2017.
- [8] Xumin pu, Shihai Shao, Kai Deng and Youxi Tang, "Effects of array orientations on degrees of freedom for 3D LoS channels in short-range communications," *IEEE Commun. Lett.*, vol. 4, no. 1, pp. 106-109, Feb. 2015.
- [9] Frode Bohagen, Pal Orte, and Geir E. Oien, "Optimal design of uniform planar antenna arrays for strong line-of-sight MIMO channels," in *Proc. IEEE 7th Workshop on Signal Processing Advances in Wireless Communications*, Cannes, France, Jul. 2006.
- [10] P. Wang, Y. Li and B. Vucetic, "Millimeter wave communications with symmetric uniform circular antenna arrays," *IEEE Commun. Lett.*, vol. 18, no. 8, pp. 1307-1310, Aug. 2014.
- [11] Liang Zhou and Yoji Ohashi, "Performance analysis of mmWave LOS-MIMO system with Uniform Circular Array," in *Proc. IEEE VTC 2015-Spring*, May. 2015.
- [12] O. Edfors and A. J. Johansson, "Is orbital angular momentum (OAM) based radio communication an unexploited area?" *IEEE Trans. Antennas and Propag.*, vol. 60, no. 2, pp. 1126-1131, Feb. 2012.
- [13] Li Zhu and Jiang Zhu, "Optimal design of uniform circular antenna array in mmWave LoS MIMO channel," *IEEE Access*, vol. 6, pp. 61022 - 61029, Sep. 2018.
- [14] Haiyue Jing, Wenchi Cheng, and Xiang-Gen Xia, "A simple channel independent beamforming scheme with parallel uniform circular array," *IEEE Communications Letters*, vol. 23, no. 3, pp. 414-417, Mar. 2019.
- [15] Yuri Jeon, Minhyun Kim, Gye-Tae Gil and Yong H. Lee, "LoS spatial multiplexing and beamforming using uniform circular array of subarrays," in *Proc. IEEE VTC 2016-Spring*, May. 2016.
- [16] W. Cheng, W. Zhang, H. Jing, S. Gao, and H. Zhang, "Orbital angular momentum for wireless communications," *IEEE Wireless Commun.*, vol. 26, no. 1, pp. 100107, Feb. 2019.
- [17] W. Zhang, S. Zheng, X. Hui, R. Dong, X. Jin, H. Chi, and X. Zhang, "Mode Division Multiplexing Communication Using Microwave Orbital Angular Momentum: An Experimental Study," *IEEE Trans. Wireless Commun.*, vol. 16, no. 2, pp. 13081318, Feb. 2017.
- [18] W. Cheng, H. Zhang, L. Liang, H. Jing, and Z. Li, "Orbital-Angular-Momentum Embedded Massive MIMO: Achieving Multiplicative Spectrum-Efficiency for mmWave Communications," *IEEE Access*, vol. 6, pp. 27322745, Dec. 2017.
- [19] Rui Chen, Hui Xu, Marco Moretti, and Jiandong Li, "Beam Steering for the Misalignment in UCA-Based OAM Communication Systems," *IEEE Wireless Commun. Lett.*, vol. 7, no. 4, pp. 582-585, Aug. 2018.
- [20] David Tse and Pramod Viswanath, *Fundamentals of Wireless Communication*, New York: Cambridge University Press, 2005.
- [21] P. Ioannides and C.A. Balanis, "Uniform circular arrays for smart antennas," *IEEE Antennas and Propagation Magazine*, vol. 47, Issue. 4, pp. 192-206, Aug. 2005.